Nano Research
2021, 14(8): 2689–2696

ISSN 1998-0124 CN 11-5974/O4
https://doi.org/10.1007/s12274-020-3273-z

Research Article

Microneedle-array patch with pH-sensitive formulation for glucose-responsive insulin delivery

Feng-Qin Luo[1,§], Guojun Chen[2,§], Wei Xu[3], Daojia Zhou[2], Jia-Xian Li[1], Yong-Cong Huang[3], Run Lin[4] (✉), Zhen Gu[2,7] (✉), and Jin-Zhi Du[1,3,5,6] (✉)

[1] *Guangzhou First People's Hospital, and Institutes for Life Sciences, School of Medicine, South China University of Technology, Guangzhou 510006, China*
[2] *Department of Bioengineering, University of California, Los Angeles, Los Angeles, CA 90095-1413, USA*
[3] *School of Biomedical Sciences and Engineering, Guangzhou International Campus, South China University of Technology, Guangzhou 510006, China*
[4] *Department of Radiology, the First Affiliated Hospital of Sun Yat-Sen University, Guangzhou 510080, China*
[5] *National Engineering Research Center for Tissue Restoration and Reconstruction, Key Laboratory of Biomedical Materials and Engineering of the Ministry of Education, Key Laboratory of Biomedical Engineering of Guangdong Province, Innovation Center for Tissue Restoration and Reconstruction, South China University of Technology, Guangzhou 510006, China*
[6] *Bioland Laboratory (Guangzhou Regenerative Medicine and Health Guangdong Laboratory), Guangzhou 510005, China*
[7] *College of Pharmaceutical Sciences, Zhejiang University, Hangzhou 310058, China*
[§] *Feng-Qin Luo and Guojun Chen contributed equally to this work.*

Received: 10 October 2020 / **Revised:** 24 November 2020 / **Accepted:** 30 November 2020

ABSTRACT

Glucose-responsive insulin delivery systems show great promise to improve therapeutic outcomes and quality of life for people with diabetes. Herein, a new microneedle-array patch containing pH-sensitive insulin-loaded nanoparticles (NPs) (SNP(I)) together with glucose oxidase (GOx)- and catalase (CAT)-loaded pH-insensitive NPs (iSNP(G+C)) is constructed for transcutaneous glucose-responsive insulin delivery. SNP(I) are prepared via double emulsion from a pH-sensitive amphiphilic block copolymer, and undergo rapid dissociation to promote insulin release at a mild acidic environment induced by GOx in iSNP(G+C) under hyperglycemic conditions. CAT in iSNP(G+C) can further consume excess H_2O_2 generated during GOx oxidation, and thus reduce the risk of inflammation toward the normal skin. The *in vivo* study on type 1 diabetic mice demonstrates that the platform can effectively regulate blood glucose levels within normal ranges for a prolonged period.

KEYWORDS

drug delivery, diabetes, glucose-responsive, pH-sensitive, microneedle

1 Introduction

Diabetes mellitus is one of the most common chronic diseases in the world, characterized by elevated blood glucose levels (BGLs) [1, 2]. According to the statistics from the International Diabetes Federation (IDF), there are about 463 million people worldwide suffering from diabetes in 2019, and the number is expected to increase to 700 million by 2045 [3]. Insulin therapy is essential for treating type 1 diabetes and advanced type 2 diabetes, and is typically administrated through subcutaneous injection [4]. However, such conventional therapy requires frequent monitoring of blood glucose via finger-prick and repeated injections, which is painful and may lead to injection phobia [5–7]. It is also challenging to accurately monitor BGLs and give precise insulin doses, which may cause severe complications, including hypoglycemia, limb amputation, blindness, and kidney failure [8, 9].

To reduce the risks described above, closed-loop insulin delivery systems have been developed as an alternative approach, aiming to intelligently mimic pancreatic functions [10–15]. Closed-loop systems can monitor BGLs automatically and "secrete" insulin in response to elevated BGLs; once BGL falls to the normal range, basal insulin release occurs. Currently, the commercial available closed-loop devices consist of a blood glucose monitor and an external insulin infusion pump [16, 17]. However, these electronic closed-loop devices with a computer-aided glucose-monitoring sensor still face many challenges including algorithm accuracy and formation of fibrosis [18, 19]. Alternatively, chemically controlled glucose-responsive closed-loop systems have been widely investigated over the last few decades [20–25]. These systems typically employ glucose-responsive elements, including glucose oxidase (GOx) [26–28], phenylboronic acid (PBA) [29–33], glucose binding proteins [34–36], and glucose transporter [37, 38], which could program the insulin release rate in response to different glucose concentrations. GOx is a glucose-specific enzyme that can convert the glucose into gluconic acid in the presence of oxygen [39]:

Address correspondence to Run Lin, linrun5@mail.sysu.edu.cn; Zhen Gu, guzhen@zju.edu.cn; Jin-Zhi Du, djzhi@scut.edu.cn

$$\text{Glucose} + O_2 + H_2O \xrightarrow{\text{GOx}} \text{Gluconic acid} + H_2O_2$$

Given the high specificity of GOx to the glucose molecule, a series of GOx-based insulin delivery systems have been reported [40, 41]. Recently, we have developed a variety of smart insulin microneedle (MN)-array patches based on the H_2O_2-responsive [42–44], hypoxia-responsive [45], or dual-responsive [46] materials. In the meantime, due to the generation of gluconic acid by GOx-mediated oxidation, a local pH decrease occurs, which provides an opportunity to develop pH-sensitive insulin delivery systems [47–49]. However, due to the strong buffering characteristics of the physiological environment, pH changes are subtle and instant. Therefore, developing materials that are capable of rapidly responding to a lightly acidic environment is advantageous for constructing GOx-based pH-responsive insulin delivery systems. Previous studies have validated that poly(2-(hexamethyleneimino) ethyl methacrylate) (PHMEMA) has ultra-pH-responsiveness and fast temporal response (< 5 ms) [50]. Therefore, it has great potential to construct pH-responsive insulin delivery systems utilizing PHMEMA.

In this study, we designed a new ultra pH-responsive MN-array patch for glucose-responsive insulin delivery. Insulin was encapsulated into the pH-sensitive nanoparticles (SNPs) (SNP(I)) made of poly(ethylene glycol)-*b*-PHMEMA (mPEG-*b*-PHMEMA). GOx was formulated in pH-insensitive NPs (iSNPs), which could minimize the leakage of enzymes. iSNPs were formed by poly(ethylene glycol)-*b*-poly(2-cyclohexylethyl methacrylate) (mPEG-*b*-PCHMA). To mitigate the toxicity concerns associated with H_2O_2 generated during glucose oxidation, catalase (CAT) was co-encapsulated in iSNPs (iSNP(G+C)). To achieve convenient and painless administration, both SNP(I) and iSNP(G+C) were loaded into the MNs. Under a hyperglycemic condition, GOx in iSNP(G+C) catalyzed the oxidation of glucose to gluconic acid, creating a local acidic environment, which triggered rapid protonation of the tertiary amino groups of the PHMEMA segments. This hydrophobic to hydrophilic transition triggered the structural disintegration of SNP(I) and led to a rapid release of insulin. Meanwhile, CAT-loaded in iSNP(G+C) can consume excess H_2O_2, and thus can reduce the risk of inflammation to the normal skin (Fig. 1).

2 Results and discussion

The amphiphilic block copolymers were prepared through reversible addition–fragmentation chain transfer (RAFT) polymerization (Fig. S1 in the Electronic Supplementary Material (ESM)). HMEMA was synthesized using $mPEG_{113}$-4-(benzenecarbonothioylsulfanyl)-4-cyanopentanoic acid (CPDB) as the chain transfer agent to obtain pH-sensitive amphiphilic block copolymer mPEG-*b*- PHMEMA. The pH-insensitive block copolymer mPEG-*b*-PCHMA was synthesized using CHMA as the monomer instead. Their chemical structures were characterized by ^{1}H nuclear magnetic resonance (NMR) (Fig. S2 in the ESM). The repeat unit of both PHMEMA and PCHMA was calculated to be 40 (Fig. S3 in the ESM).

Insulin-loaded SNP(I) and GOx/CAT-loaded iSNP(G+C) were prepared via double emulsion-solvent evaporation. As measured by dynamic light scattering (DLS), the average size of SNP(I) was around 120 nm, which was slightly smaller than iSNP(G+C) (~ 136 nm) (Figs. 2(a) and 2(c)), probably due to the variable molecular sizes and loading levels of the payloads. Transmission electron microscopy (TEM) images showed that both SNP(I) and iSNP(G+C) had a spherical shape (Figs. 2(b) and 2(d)). The load level of insulin in SNP(I) was 5 wt%. The weight ratio of GOx and CAT in iSNP(G+C) was set at 4:1 [27].

To demonstrate pH responsiveness, SNP(I) was incubated in phosphate buffered saline (PBS) solutions of different pH values. As shown in Fig. 3(a), the size of SNP(I) decreased sharply around pH 6.5, indicating dissociation of SNP(I) due to the hydrophobic to hydrophilic transition of PHMEMA segments at pH 6.5. In contrast, the size of iSNP(G+C) remained constant regardless of pH changes (Fig. 3(b)). To confirm pH decrease upon GOx under different glucose concentrations, we measured pH changes of the solutions with a glucose concentration of 100 or 400 mg/dL in the presence of GOx (0.2 mg/mL). As shown in Fig. S4 in the ESM, the pH of the solution with a glucose concentration of 400 mg/dL dropped sharply within 2 h, while the pH did not change significantly under normoglycemic levels (100 mg/dL). It suggests that the gluconic acid is generated in a glucose concentration-dependent manner. We then investigated the size changes of SNP(I) under various glucose concentrations. As shown in Fig. 3(c), the hydrodynamic

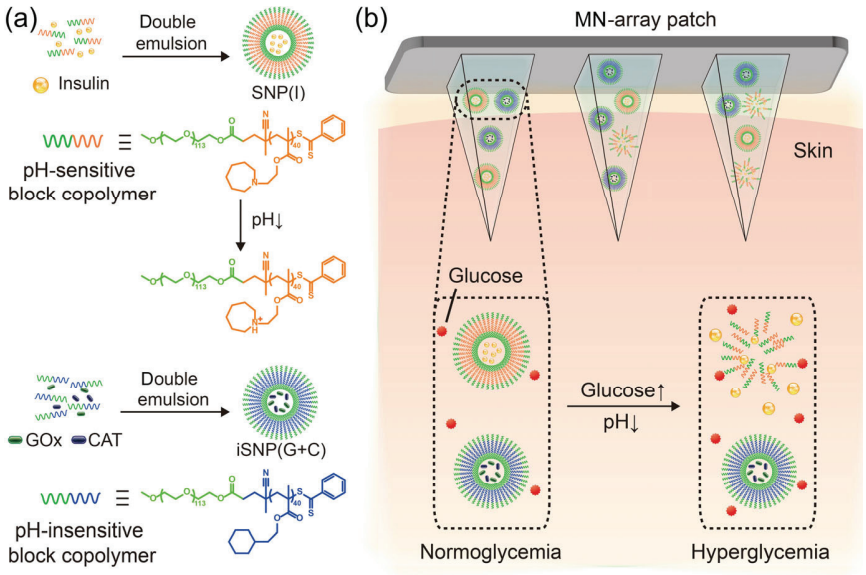

Figure 1 Scheme of MN-array patch integrated with pH-sensitive insulin nanoformulations for glucose-responsive insulin delivery. (a) The chemical structure and formation of SNP(I) and iSNP(G+C). (b) Schematic illustration of the MN-array patch loaded with SNP(I) and iSNP(G+C) for *in vivo* insulin delivery triggered by a hyperglycemic state to release more insulin.

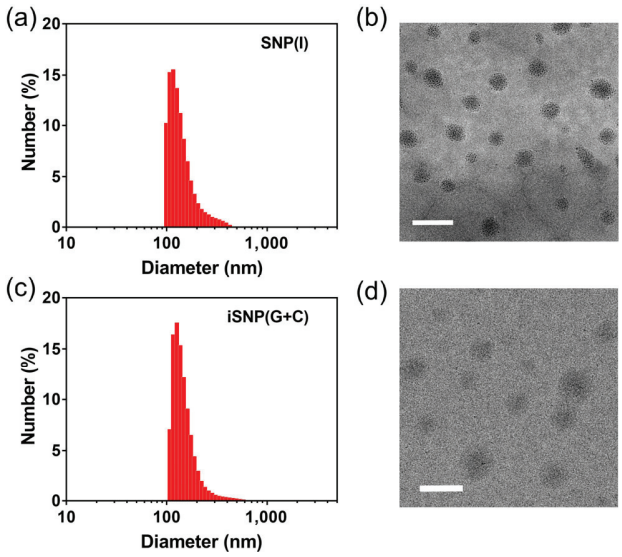

Figure 2 (a) Hydrodynamic size and (b) TEM image of SNP(I). (c) Hydrodynamic size and (d) representative TEM image of iSNP(G+C). Scale bar: 200 nm.

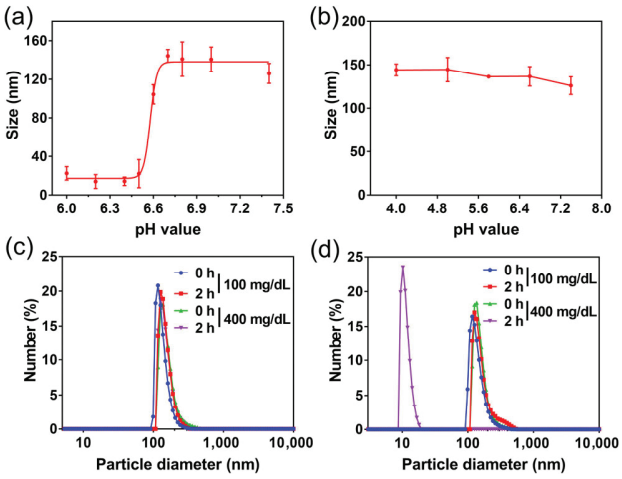

Figure 3 DLS measurement of size changes of SNP(I) (a) and iSNP(G+C) (b) in PBS buffers of various pH values. Data points are means ± standard deviation (SD) (n = 3). Hydrodynamic size of SNP(I) incubated in various glucose concentrations without (c) or with GOx (0.2 mg/mL) (d) over time.

size of SNP(I) incubated in different glucose concentrations (100 or 400 mg/dL) without GOx remained unchanged over time. However, when GOx (0.2 mg/mL) was added, the size of SNP(I) incubated in higher glucose concentration (400 mg/dL) decreased obviously over time, indicating that SNP(I) could be dissociated in response to pH changes induced by GOx upon hyperglycemia (Fig. 3(d)).

We further evaluated the glucose-responsive insulin release capability of SNP(I). SNP(I) were incubated in PBS with various glucose concentrations, including a control level (0 mg/dL), a normoglycemic level (100 mg/dL), and a hyperglycemic level (400 mg/dL). Consistent with the size changes of SNP(I), at a hyperglycemic level, more than 90% of insulin was released within 4 h, whereas only about 30% was released at normoglycemic level (Fig. 4(a)). Furthermore, the release rates significantly increased when the glucose concentration increased from 100 to 400 mg/dL, indicating that the amount of insulin released was glucose concentration-dependent (Fig. 4(b)). Furthermore, a pulsatile release profile of insulin was observed when SNP(I) were alternatively incubated in hyperglycemic (400 mg/dL) and normoglycemic (100 mg/dL) levels (Fig. 4(c)). Additionally, the circular dichroism (CD) spectrum showed that the insulin released from SNP(I) maintained a secondary conformational structure (Fig. 4(d)). GOx and CAT were encapsulated in the pH-insensitive NPs to minimize the leakage of these two enzymes. To evaluate the release kinetics of GOx and CAT from iSNP(G+C) under different pH conditions, we labeled the GOx with rhodamine B (RhB) and the CAT with fluorescein isothiocyanate (FITC), and constructed the standard curves (Fig. S5 in the ESM). As expected, the minimal amounts of GOx and CAT were released, which were also independent of pH values (Figs. 4(e) and 4(f)). Although a small portion of enzymes is released, they are expected to enter the bloodstream and quickly be metabolized [39, 51].

Next, we loaded SNP(I) and iSNP(G+C) into a MN-array patch for painless and convenient administration. The MN array patch was prepared via micromolding [45, 52]. Briefly, SNP(I) and iSNP(G+C) were first loaded in microcavities of a silicone mold under vacuum, followed by the addition of a polyvinylpyrrolidone (PVP) solution. After complete drying, the MN-array patch was peeled off from the mold. An array of 15 × 15 pyramid-shaped MNs, with each MN with 700 μm height and 600 μm center to center space, was used for all tests. Scanning electron microscopy (SEM) images confirmed the formation of MN arrays (Fig. 5(a)). PVP was chosen as the main MN matrix because it is highly biocompatible and exhibits a suitable mechanical property [52]. Measurement of mechanical strength suggested a failure force for the MNs to be 0.62 N/needle, demonstrating sufficient strength for skin insertion, which was also validated by trypan-blue-staining test on the mouse skin (Fig. 5(b)). The fluorescence image of MNs that contained RhB-insulin–loaded SNP(I) indicated that SNP(I) were mostly distributed inside the needle tips (Figs. 5(c) and 5(d)).

We evaluate the *in vivo* performance of MN-array patches in the streptozotocin (STZ)-induced type 1 diabetic mice (Fig. S6 in the ESM). The mice were divided into five groups treated with (1) blank MN-array patches as control; (2) MN-array patches loaded with SNP(I) (MN-(SNP(I)); (3) MN-array patches loaded with insulin-loaded pH-insensitive NPs (iSNP(I)) and GOx-loaded pH-insensitive NPs (iSNP(G)) (MN-(iSNP(I) + iSNP(G)); (4) MN-array patches loaded with SNP(I) and iSNP(G) (MN-(SNP(I) + iSNP(G)); (5) and MN-array patches loaded with SNP(I) and iSNP(G+C) (MN-(SNP(I) + iSNP(G+C)). The BGLs of each group were monitored over time after administration. As shown in Fig. 6(a), the BGLs of mice treated with MN-(SNP(I) + iSNP(G) and MN-(SNP(I) + iSNP(G+C)) decreased to normoglycemic level and maintained below 200 mg/dL for 8 h (Fig. 6(b)). In contrast, the BGLs of mice treated with MN-(SNP(I)) that do not contain the GOx decreased at the beginning but returned to the hyperglycemic level quickly, which was mainly ascribed to the basal insulin release from MN-(SNP(I)). The mice treated with MNs loaded with iSNP(I) and iSNP(G) showed no obvious BGLs reduction. In sum, these observations confirmed that the glucose-responsive insulin release was based on the oxidation of glucose catalyzed by GOx resulting in the decrease of local pH to trigger the dissociation of SNP(I). To further investigate the glucose-responsiveness of MN-(SNP(I) + iSNP(G+C)), an intraperitoneal glucose tolerance test (IPGTT) was carried out 3 h post-administration of MNs. As shown in Fig. 6(c), insulin showed an obvious increase followed by the increase of BLGs due to glucose challenge, indicating a fast glucose-responsive property of MN-(SNP(I) + iSNP(G+C)).

We then accessed the biocompatibility of the MN patch. As shown in Fig. S7 in the ESM, no obvious body weight changes

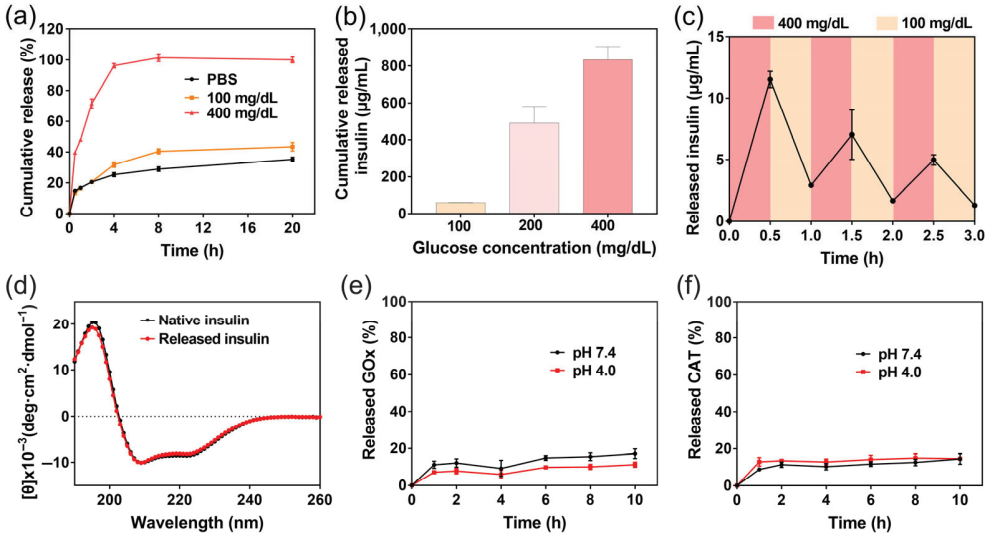

Figure 4 (a) *In vitro* glucose-dependent insulin release from SNP(I) with various glucose concentrations at 37 °C in the presence of GOx (0.2 mg/mL). (b) Cumulative insulin release profile of SNP(I). The NPs were incubated in each solution for 30 min. (c) Pulsatile release profile of SNP(I) at different glucose concentration (100 and 400 mg/dL). (d) CD spectra of native insulin and insulin released from SNP(I). (e) and (f) *In vitro* GOx (e) and CAT (f) release from iSNP(G+C) under different pH conditions over time. Data points are means ± SD (n = 3).

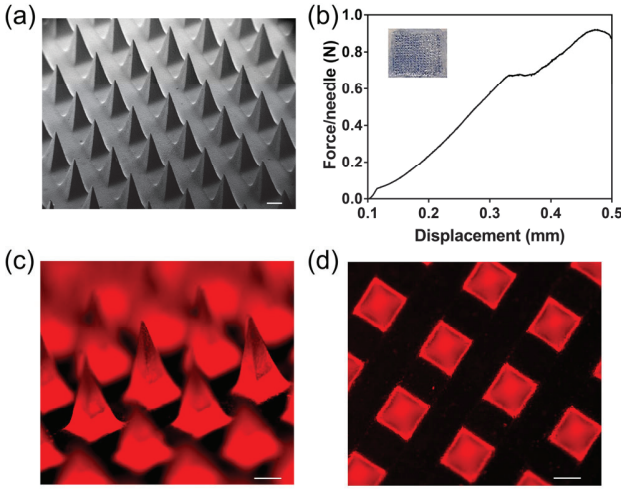

Figure 5 (a) A representative scanning electron microscopy (SEM) image of the MN-array patch. (b) Mechanical behaviors of the MNs. Inset is a representative image of trypan blue staining of mouse skin transcutaneously treated with a MN-array patch. (c) and (d) Representative fluorescence microscopy images of the MN-array patch loaded with RhB-labeled insulin NPs, side-view (c), and bottom view (d). Scale bar: 200 μm.

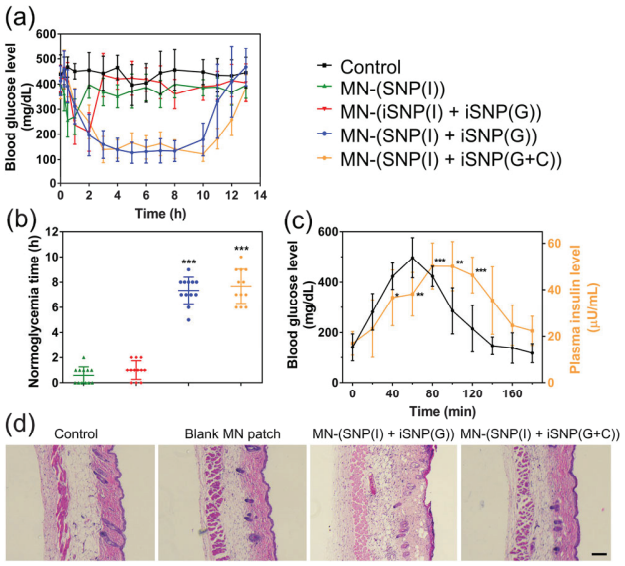

Figure 6 (a) Blood glucose levels of type 1 diabetic mice after treatment with blank MNs as control, MNs loaded with SNP(I), MNs loaded with iSNP(I) and iSNP(G), MNs loaded with SNP(I) and iSNP(G), MNs loaded with SNP(I) and iSNP(G+C). Data points are means ± SD (n = 12). (b) Normoglycemic time of mice treated with various MN-array patches. Data points are means ± SD (n = 12). Statistical significance was calculated by comparison with group treated with MN-SNP(I). (c) *In vivo* glucose-responsive insulin release triggered by intraperitoneal glucose injection at 3 h after treatment with MN-(SNP(I) + iSNP(G+C)). Data points are means ± SD (n = 4). Statistical significance was calculated by comparison with values at 0 min. (d) H&E staining of skins of treated with blank MN patch, MNs-(SNP(I) + iSNP(G)) and MNs-(SNP(I) + iSNP(G+C)). Scale bar, 50 μm. All the statistical analyses were performed by one-way analysis of variance (ANOVA). *p < 0.05, **p < 0.01, and ***p < 0.001.

were observed during or after MN-(SNP(I) + iSNP(G+C)) treatment. Furthermore, the hematoxylin and eosin (H&E) staining analyses were performed on the skin after application with the MN patch. Compared with the skin treated with blank MN, the skin samples treated with MN-(SNP(I) + iSNP(G)) showed apparent neutrophil infiltration, suggesting a pathophysiological response and tissue inflammation induced by H_2O_2. Nevertheless, reduced neutrophil infiltration was found in skin samples that were treated with MN-(SNP(I) + iSNP(G+C)) (Fig. 6(d)). These results indicated that CAT could effectively mitigate the H_2O_2-associated toxicity in the GOx-based systems.

3 Conclusions

In summary, we have developed a new glucose-responsive insulin MN patch system integrating pH-responsive insulin nanoformulations. A local acid environment can be generated due to the production of gluconic acid during the oxidation process of glucose under hyperglycemic levels, which facilitates a rapid protonation of the tertiary amine in the SNPs, resulting in the dissociation of NPs and insulin release. Furthermore, encapsulation of GOx and CAT in the pH-insensitive NPs can prevent the leakage of enzymes and inhibit the toxicity issues associated with the byproduct H_2O_2. *In vivo* experiments indicated

that MN loaded with SNP(I) and iSNP(G+C) exhibited excellent regulation of BGLs with fast responsiveness. This MN-array patch with ultra pH-sensitive formulation promises a potential strategy for designing a closed-loop insulin delivery system to treat type 1 and advanced type 2 diabetes. Future efforts, including the optimization in large animal models, scale up and manufacturing, should be taken into consideration for potential translation of this formulation. Furthermore, the concept of this glucose-responsive MN array patch can also extended to applications associated with glucose/pH-responsive drug delivery for treating different diseases.

4 Experimental

4.1 Materials

Poly(ethylene glycol) methyl ether (mPEG$_{113}$-OH, M_n = 5,000 Da), PVP (M_W = 360 kDa), GOx and CAT were purchased from Sigma-Aldrich. Methacryloyl chloride, *N*-(2-hydroxyethyl)hexamethyleneimine, hydroquinone, and CPDB were purchased from Sun Chemical Technology Co., Ltd. (Shanghai, China). 2-cyclohexylethanol was purchased from Xian-Dinn Biotech Co., Ltd. (Shanghai, China). 2,2-azobis(2-methylpropionitrile) (AIBN), RhB, FITC, 4-dimethylaminopyridine (DMAP), and *N*,*N*'-dicyclohexylcarbodiimide (DCC) were purchased from Shanghai Aladdin Bio-Chem Technology Co., Ltd (Shanghai, China). Other chemicals were purchased from Sinopharm Chemical Reagent Co., Ltd and used as received unless otherwise specified.

4.2 Characterizations

^{1}H NMR spectra were recorded on a Bruker AV400 NMR spectrometer (Bruker Corporation, Switzerland) using $CDCl_3$ as a solvent. Particle size measurements were conducted using Anton Paar Litesizer 500 Particle Analyzer (Anton Paar Corporation, Austria). Morphology of NPs was displayed by Thermo Scientific Talos L120C transmission electron microscopy (Thermo Scientific, USA). pH of solutions were recorded using a FE-28 pH meter (Mettler Toledo, China). The concentration of insulin, GOx and CAT labeled with fluorescent molecules were recorded using Shimadzu RF-6000 spectrophotometer (Shimadzu, Japan).

4.3 Synthesis of poly(ethylene glycol) dithiobenzoate (mPEG$_{113}$-CPDB) chain transfer agent

mPEG$_{113}$-OH was azeotropic with toluene to remove water before use. mPEG$_{113}$-OH (4.739 g), CPDB (0.519 g) and DMAP (0.029 g) were dissolved in anhydrous dichloromethane (30 mL) in a three-neck round flask under nitrogen. A solution of DCC (0.548 g) in anhydrous dichloromethane (10 mL) was then added dropwise under stirring, cooled with an ice-water bath. The mixture was then gradually warmed to room temperature and stirred for 12 h. Then, the solution was poured into excess diethyl ether to obtain pink precipitate. The precipitation process was repeated for an additional two times. The product was obtained as pink solid. Yield: 92%.

4.4 Synthesis of HMEMA

N-(2-hydroxyethyl)hexamethyleneimine (7.152 g), triethylamine (5.566 g), and inhibitor hydroquinone (0.055 g) were dissolved in anhydrous tetrahydrofuran (THF). Then, methacryloyl chloride (5.487 g) in anhydrous THF was added and stirred overnight. The reaction solution was filtered and concentrated using a rotary evaporator. The product was obtained as a colorless liquid through distillation under vacuum. Yield: 78%.

4.5 Synthesis of CHMA

CHMA was synthesized following the same method as HMEMA by replacing *N*-(2-hydroxyethyl)hexamethyleneimine with 2-cyclohexylethanol. The product was obtained as a colorless liquid through distillation under vacuum. Yield: 80%.

4.6 Synthesis of mPEG-*b*-PHMEMA by RAFT

Briefly, mPEG$_{113}$-CPDB (230.4 mg), HMEMA (554.4 mg), and AIBN (2.4 mg) were added to a polymerization tube. Anhydrous dioxane (1.3 mL) was then added to dissolve the monomer and initiator. After three cycles of freeze-pump-thaw to remove oxygen, the polymerization was carried out at 75 °C for 10 h. The mixture was then precipitated into cold hexane. The precipitate was dried overnight in vacuum, the product was obtained as a yellow solid in 90% yield. The degree of polymerization of PHMEMA block was 40 according to ^{1}H NMR spectrum.

4.7 Synthesis of mPEG-*b*-PCHMA by RAFT

Block copolymer mPEG-*b*-PCHMA was synthesized by RAFT polymerization following the same method as mPEG-*b*-PHMEMA by replacing HMEMA with CHMA. The product was obtained as a pink solid in 85% yield. The degree of polymerization of PCHMA block was 40 according to ^{1}H NMR spectrum.

4.8 Synthesis of FITC-insulin, RhB-GOx, and FITC-CAT

Briefly, 40 mg of insulin (GOx or CAT) was dissolved in Na_2CO_3 buffer (2 mL, 20 mM, pH 8.5). Then, 0.5 mg of fluorescence isothiocyanate dyes (FITC or RhB) in dimethyl sulfoxide (DMSO) was added dropwise. The mixture was stirred at room temperature overnight. The unreacted dyes were removed by ultrafiltration.

4.9 Preparation of SNP(I) or iSNP(G+C)

SNP(I) were prepared by double emulsion-solvent evaporation. Typically, an aqueous solution of insulin (1 mg) in 20 μL of distilled water was emulsified by sonication for 1 min over an ice bath in 0.2 mL of chloroform containing 10 mg of mPEG-*b*-PHMEMA. The primary emulsion was then emulsified in 5 mL of distilled water by sonication (80 W for 2 min) over an ice bath to form a W/O/W emulsion. After removal of the organic solvents, the nanoparticles were collected by centrifugation (20,000× g, 20 min) and were washed twice to remove free insulin. iSNP(G+C) were prepared following the same method with SNP(I). Briefly, the mixed solution of GOx and CAT (1 mg of protein in 10 μL distilled water, w:w=4:1) was emulsified in 0.1 mL of chloroform containing 5 mg of mPEG-*b*-CHMA. Then, 5 mL of distilled water was added and further emulsified for 2 min. The nanoparticles were collected by centrifugation (20,000× g, 20 min) and were washed twice to remove free enzymes.

4.10 *In vitro* FITC-insulin release from the SNP(I)

SNP(I) were suspended in 10 mM PBS at pH 7.4 and allocated to centrifuge tubes. Various amounts of glucose (0, 100, or 400 mg/dL final concentration) and GOx (0.2 mg/mL) were added to the solutions. At predetermined time intervals, the solution was centrifuged to collect supernatant (100 μL each tube) for fluorescence quantification. To assess the self-regulated insulin release profile, the SNP(I) and iSNP(G+C) (GOx: 0.2 mg/mL) were first incubated in 1 mL of 400 mg/dL glucose

solution for 30 min at 37 °C. The sample was then centrifuged at 20,000× g for 10 min, and all of the supernatant was recovered. Next, the sample was incubated in 1 mL of 100 mg/dL glucose solution for another 30 min. After centrifugation, all of the supernatant was recovered. This cycle was repeated for three cycles. The release insulin was determined using a spectrophotometer.

4.11 *In vitro* RhB-GOx or FITC-CAT release from the iSNP(G+C)

To assess the GOx (CAT) release profile from pH-insensitive nanoparticles, iSNP(G+C) were incubated in PBS solution under different pH values (7.4 and 4.0). At the determined time interval, solution was centrifuged to collect supernatant (100 μL each tube) and replaced with 100 μL fresh PBS solution. The concentration of GOx (CAT) was determined using the spectrophotometer.

4.12 Fabrication of SNP(I)- and iSNP(G+C)-loaded MNs

Silicone micromolds were purchased from Blueacre Technology Ltd. The MNs were arranged in a 15 × 15 array with 600 μm center-to-center spacing with a MN height of 700 μm. SNP(I) (4 mg) and iSNP(G+C) (0.8 mg) in 200 μL of DI water was deposited onto the MN mold surface. Molds were then placed under vacuum for 30 min. Thereafter, 1 mL of PVP solution (10 wt%) was deposited on the molds and dried at room temperature overnight. After completely desiccation, the MN-array patch was separated from the silicone mold. The resulting MN-array patches were stored under vacuum for later study.

4.13 Mechanical strength test

The mechanical strength of MNs was tested on an Instron tensile testing machine. The initial gauge was set as about 2 mm between MNs and the stainless-steel plate. The speed of the plate movement toward MNs was set at 0.1 mm/min.

4.14 *In vivo* studies on STZ-induced diabetic mice

STZ-induced diabetic mice were purchased from the Jackson Laboratory, USA. The animal protocol was approved by the Institutional Animal Care and Use Committee at UCLA. The blood glucose levels of mice were measured via tail vein blood samplings using a Clarity GL2Plus glucose meter. The mice were divided into five groups and applied with (1) blank MN-array patches as control; (2) MN-array patches with SNP(I) (MN-(SNP(I)); (3) MN-array patches with insulin-loaded pH-insensitive NPs (iSNP(I)) and GOx-loaded pH-insensitive NPs (iSNP(G)) (MN-(iSNP(I) + iSNP(G)); (4) MN-array patches with SNP(I) and iSNP(G) (MN-(SNP(I) + iSNP(G)); (5) and MN-array patches loaded SNP(I) and iSNP(G+C) (MN-(SNP(I) + iSNP(G+C)). The insulin dose was 10 mg/kg. The blood glucose levels were monitored over time.

An IPGTT was performed to study the glucose responsiveness of the MN patches *in vivo* 3 h post application. Briefly, mice were applied with MN-(SNP(I) + iSNP(G+C) with insulin dose of 10 mg/kg for each mouse for 3 h. Thereafter, a glucose solution in PBS with a dose of 1.5 g/kg was intraperitoneally injected into the mice. The blood glucose levels were monitored over time. To measure the plasma insulin levels *in vivo*, 25 μL of blood sample was collected at indicated time points. The plasma insulin levels were measured via a Human Insulin ELISA kit (Calbiotech, USA).

4.15 Biocompatibility analysis

The biocompatibility of MN-array patches was assessed 2 days post administration. The MN-patch-applied skin tissues of mice were excised. The skin were fixed in 10% formalin and cut into 50-μm sections, which were further stained using H&E for histological analysis.

4.16 Statistical analysis

Statistical analyses were performed via either the Student's *t*-test or an ANOVA test as indicated in the figure captions.

Acknowledgements

This work was supported by National Key R&D Program of China (No. 2017YFA0205600), National Natural Science Foundation of China (Nos. 31771091 and 51922043), Guangdong Natural Science Funds for Distinguished Young Scholar (No. 2017A030306018), Guangdong Provincial Programs (Nos. 2017ZT07S054 and 2017GC010304), Outstanding Scholar Program of Bioland Laboratory (Guangzhou Regenerative Medicine and Health Guangdong Laboratory) (No. 2018GZR110102001), Guangdong Natural Science Foundation (No. 2018A030310285), Science and Technology Program of Guangzhou (Nos. 201902020018, 201804020060, and 201904010398), and Fundamental Research Funds for Central Universities, National Science Foundation (No. 1919285) and American Diabetes Association (No. 1-15-ACE-21).

Electronic Supplementary Material: Supplementary materials (^{1}H NMR spectra of HMEMA monomer, CHMA monomer and block copolymers, the standard curves of GOx-RhB and CAT-FITC) is available in the online version of this article at https://doi.org/10.1007/s12274-020-3273-z.

References

[1] Chatterjee, S.; Khunti, K.; Davies, M. J. Type 2 diabetes. *Lancet*, **2017**, *389*, 2239–2251.

[2] Atkinson, M. A.; Eisenbarth, G. S.; Michels, A. W. Type 1 diabetes. *Lancet*, **2014**, *383*, 69–82.

[3] International Diabetes Federation. *IDF Diabetes Atlas*, *9th edition 2019* [Online]. Brussels, Belgium: Internationa Diabetes Federation, 2019. https://www.diabetesatlas.org (accessed Oct 10, 2020).

[4] Owens, D. R.; Zinman, B.; Bolli, G. B. Insulins today and beyond. *Lancet*, **2001**, *358*, 739–746.

[5] Bluestone, J. A.; Herold, K.; Eisenbarth, G. Genetics, pathogenesis and clinical interventions in type 1 diabetes. *Nature*, **2010**, *464*, 1293–1300.

[6] Karges, B.; Binder, E.; Rosenbauer, J. Complications with insulin pump therapy vs insulin injection therapy-reply. *JAMA*, **2018**, *319*, 503–504.

[7] Yeh, H. C.; Brown, T. T.; Maruthur, N.; Ranasinghe, P.; Berger, Z.; Suh, Y. D.; Wilson, L. M.; Haberl, E. B.; Brick, J.; Bass, E. B. et al. Comparative effectiveness and safety of methods of insulin delivery and glucose monitoring for diabetes mellitus: A systematic review and meta-analysis. *Ann. Intern. Med.*, **2012**, *157*, 336–347.

[8] Writing Team for the Diabetes Control; Complications Trial/Epidemiology of Diabetes Interventions; Complications Research Group. Sustained effect of intensive treatment of type 1 diabetes mellitus on development and progression of diabetic nephropathy: The epidemiology of diabetes interventions and complications (EDIC) study. *JAMA*, **2003**, *290*, 2159–2167.

[9] Donnelly, L. A.; Morris, A. D.; Frier, B. M.; Ellis, J. D.; Donnan, P. T.; Durrant, R.; Band, M. M.; Reekie, G.; Leese, G. P.; DARTS/MEMO Collaboration. Frequency and predictors of hypoglycaemia in Type 1 and insulin-treated Type 2 diabetes: A population-based study. *Diabet. Med.*, **2005**, *22*, 749–755.

[10] Shen, D.; Yu, H. J.; Wang, L.; Khan, A.; Haq, F.; Chen, X.; Huang, Q.; Teng, L. S. Recent progress in design and preparation of glucose-responsive insulin delivery systems. *J. Control. Release*, **2020**, *321*, 236–258.
[11] Yu, J. C.; Zhang, Y. Q.; Yan, J. J.; Kahkoska, A. R.; Gu, Z. Advances in bioresponsive closed-loop drug delivery systems. *Int. J. Pharm.*, **2018**, *544*, 350–357.
[12] Bakh, N. A.; Cortinas, A. B.; Weiss, M. A.; Langer, R. S.; Anderson, D. G.; Gu, Z.; Dutta, S.; Strano, M. S. Glucose-responsive insulin by molecular and physical design. *Nat. Chem.,* **2017**, *9*, 937–944.
[13] Ravaine, V.; Ancla, C.; Catargi, B. Chemically controlled closed-loop insulin delivery. *J. Control. Release*, **2008**, *132*, 2–11.
[14] Jamaledin, R.; Makvandi, P.; Yiu, C. K. Y.; Agarwal, T.; Vecchione, R.; Sun, W. J.; Maiti, T. K.; Tay, F. R.; Netti, P. A. Engineered microneedle patches for controlled release of active compounds: recent advances in release profile tuning. *Adv. Ther.*, **2020**, in press, https://doi.org/10.1002/adtp.202000171.
[15] Jamaledin, R.; Yiu, C. K. Y.; Zare, E. N.; Niu, L. N.; Vecchione, R.; Chen, G. J.; Gu, Z.; Tay, F. R.; Makvandi, P. Advances in antimicrobial microneedle patches for combating infections. *Adv. Mater.*, **2020**, *32*, 2002129.
[16] Steil, G. M.; Rebrin, K.; Darwin, C.; Hariri, F.; Saad, M. F. Feasibility of automating insulin delivery for the treatment of type 1 diabetes. *Diabetes*, **2006**, *55*, 3344–3350.
[17] Chen, X.; Wang, L.; Yu, H. J.; Li, C. J.; Feng, J. Y.; Haq, F.; Khan, A.; Khan, R. U. Preparation, properties and challenges of the microneedles-based insulin delivery system. *J. Control. Release*, **2018**, *288*, 173–188.
[18] Veiseh, O.; Tang, B. C.; Whitehead, K. A.; Anderson, D. G.; Langer, R. Managing diabetes with nanomedicine: Challenges and opportunities. *Nat. Rev. Drug Discov.*, **2015**, *14*, 45–57.
[19] Weissberg-Benchell J.; Antisdel-Lomaglio J.; Seshadri R. Insulin pump therapy: A meta-analysis. *Diabetes Care*, **2003**, *26*, 1079–1087.
[20] Wang, J. Q.; Wang, Z. J.; Yu, J. C.; Kahkoska, A. R.; Buse, J. B.; Gu, Z. Glucose-responsive insulin and delivery systems: Innovation and translation. *Adv. Mater.*, **2020**, *32*, 1902004.
[21] Zhang, Y. Q.; Yu, J. C.; Kahkoska, A. R.; Wang, J. Q.; Buse, J. B.; Gu, Z. Advances in transdermal insulin delivery. *Adv. Drug Deliv. Rev.*, **2019**, *139*, 51–70.
[22] Gordijo, C. R.; Koulajian, K.; Shuhendler, A. J.; Bonifacio, L. D.; Huang, H. Y.; Chiang, S.; Ozin, G. A.; Giacca, A.; Wu, X. Y. Nanotechnology-enabled closed loop insulin delivery device: *In vitro* and *in vivo* evaluation of glucose-regulated insulin release for diabetes control. *Adv. Funct. Mater.*, **2011**, *21*, 73–82.
[23] Jin, X.; Zhu, D. D.; Chen, B. Z.; Ashfaq, M.; Guo, X. D. Insulin delivery systems combined with microneedle technology. *Adv. Drug Deliv. Rev.*, **2018**, *127*, 119–137.
[24] Wu, Q.; Wang, L.; Yu, H. J.; Wang, J. J.; Chen, Z. F. Organization of glucose-responsive systems and their properties. *Chem. Rev.*, **2011**, *111*, 7855–7875.
[25] Yu, J. C.; Zhang, Y. Q.; Wang, J. Q.; Wen, D.; Kahkoska, A. R.; Buse, J. B.; Gu, Z. Glucose-responsive oral insulin delivery for postprandial glycemic regulation. *Nano Res.*, **2019**, *12*, 1539–1545.
[26] Gu, Z.; Dang, T. T.; Ma, M. L.; Tang, B. C.; Cheng, H.; Jiang, S.; Dong, Y. Z.; Zhang, Y. L.; Anderson, D. G. Glucose-responsive microgels integrated with enzyme nanocapsules for closed-loop insulin delivery. *ACS Nano*, **2013**, *7*, 6758–6766.
[27] Gu, Z.; Aimetti, A. A.; Wang, Q.; Dang, T. T.; Zhang, Y. L.; Veiseh, O.; Cheng, H.; Langer, R. S.; Anderson, D. G. Injectable nano-network for glucose-mediated insulin delivery. *ACS Nano*, **2013**, *7*, 4194–4201.
[28] Podual, K.; Doyle, F. J.; Peppas, N. A. Glucose-sensitivity of glucose oxidase-containing cationic copolymer hydrogels having poly (ethylene glycol) grafts. *J. Control. Release*, **2000**, *67*, 9–17.
[29] Chou, D. H. C.; Webber, M. J.; Tang, B. C.; Lin, A. B.; Thapa, L. S.; Deng, D.; Truong, J. V.; Cortinas, A. B.; Langer, R.; Anderson, D. G. Glucose-responsive insulin activity by covalent modification with aliphatic phenylboronic acid conjugates. *Proc. Natl. Acad. Sci. USA*, **2015**, *112*, 2401–2406.
[30] Huang, Q.; Wang, L.; Yu, H. J.; Ur-Rahman, K. Advances in phenylboronic acid-based closed-loop smart drug delivery system for diabetic therapy. *J. Control. Release*, **2019**, *305*, 50–64.
[31] Yu, J. C.; Wang, J. Q.; Zhang, Y. Q.; Chen, G. J.; Mao, W. W.; Ye, Y. Q.; Kahkoska, A. R.; Buse, J. B.; Langer, R.; Gu, Z. Glucose-responsive insulin patch for the regulation of blood glucose in mice and minipigs. *Nat. Biomed. Eng.*, **2020**, *4*, 499–506.
[32] Matsumoto, A.; Tanaka, M.; Matsumoto, H.; Ochi, K.; Moro-oka, Y.; Kuwata, H.; Yamada, H.; Shirakawa, I.; Miyazawa, T.; Ishii, H. et al. Synthetic "smart gel" provides glucose-responsive insulin delivery in diabetic mice. *Sci. Adv.*, **2017**, *3*, eaaq0723.
[33] Matsumoto, A.; Ishii, T.; Nishida, J.; Matsumoto, H.; Kataoka, K.; Miyahara, Y. A synthetic approach toward a self-regulated insulin delivery system. *Angew. Chem., Int. Ed.*, **2012**, *51*, 2124–2128.
[34] Wu, S. S.; Huang, X.; Du, X. Z. Glucose-and pH-responsive controlled release of cargo from protein-gated carbohydrate-functionalized mesoporous silica nanocontainers. *Angew. Chem., Int. Ed.*, **2013**, *52*, 5580–5584.
[35] Wang, J. Q.; Yu, J. C.; Zhang, Y. Q.; Zhang, X. D.; Kahkoska, A. R.; Chen, G. J.; Wang, Z. J.; Sun, W. J.; Cai, L. L.; Chen, Z. W. et al. Charge-switchable polymeric complex for glucose-responsive insulin delivery in mice and pigs. *Sci. Adv.*, **2019**, *5*, eaaw4357.
[36] Yu, J. C.; Zhang, Y. Q.; Sun, W. J.; Kahkoska, A. R.; Wang, J. Q.; Buse, J. B.; Gu, Z. Insulin-responsive glucagon delivery for prevention of hypoglycemia. *Small*, **2017**, *13*, 1603028.
[37] Wang, C.; Ye, Y. Q.; Sun, W. J.; Yu, J. C.; Wang, J. Q.; Lawrence, D. S.; Buse, J. B.; Gu, Z. Red blood cells for glucose-responsive insulin delivery. *Adv. Mater.*, **2017**, *29*, 1606617.
[38] Wang, J. Q.; Yu, J. C.; Zhang, Y. Q.; Kahkoska, A. R.; Wang, Z. J.; Fang, J.; Whitelegge, J. P.; Li, S.; Buse, J. B.; Gu, Z. Glucose transporter inhibitor-conjugated insulin mitigates hypoglycemia. *Proc. Natl. Acad. Sci. USA*, **2019**, *116*, 10744–10748.
[39] Bankar, S. B.; Bule, M. V.; Singhal, R. S.; Ananthanarayan, L. Glucose oxidase–An overview. *Biotechnol. Adv.*, **2009**, *27*, 489–501.
[40] Zhang, G. Y.; Ji, Y.; Li, X. L.; Wang, X. Y.; Song, M. M.; Gou, H. L.; Gao, S.; Jia, X. D. Polymer-covalent organic frameworks composites for glucose and pH dual-responsive insulin delivery in mice. *Adv. Healthc. Mater.*, **2020**, *9*, 2000221.
[41] Zuo, M. Z.; Qian, W. R.; Xu, Z. Q.; Shao, W.; Hu, X. Y.; Zhang, D. M.; Jiang, J. L.; Sun, X. Q.; Wang, L. Y. Multiresponsive supramolecular theranostic nanoplatform based on pillar[5]arene and diphenylboronic acid derivatives for integrated glucose sensing and insulin delivery. *Small*, **2018**, *14*, 1801942.
[42] Hu, X. L.; Yu, J. C.; Qian, C. G; Lu, Y.; Kahkoska, A. R.; Xie, Z. G.; Jing, X. B.; Buse, J. B.; Gu, Z. H_2O_2-responsive vesicles integrated with transcutaneous patches for glucose-mediated insulin delivery. *ACS Nano*, **2017**, *11*, 613–620.
[43] Zhang, Y. Q.; Wang, J. Q.; Yu, J. C.; Wen, D.; Kahkoska, A. R.; Lu, Y.; Zhang, X. D.; Buse, J. B.; Gu, Z. Bioresponsive microneedles with a sheath structure for H_2O_2 and pH cascade-triggered insulin delivery. *Small*, **2018**, *14*, 1704181.
[44] Wang, J. Q.; Ye, Y. Q.; Yu, J. C.; Kahkoska, A. R.; Zhang, X. D.; Wang, C.; Sun, W. J.; Corder, R. D.; Chen, Z. W.; Khan, S. A. et al. Core–shell microneedle gel for self-regulated insulin delivery. *ACS Nano*, **2018**, *12*, 2466–2473.
[45] Yu, J. C.; Zhang, Y. Q.; Ye, Y. Q.; DiSanto, R.; Sun, W. J.; Ranson, D.; Ligler, F. S.; Buse, J. B.; Gu, Z. Microneedle-array patches loaded with hypoxia-sensitive vesicles provide fast glucose-responsive insulin delivery. *Proc. Natl. Acad. Sci. USA*, **2015**, *112*, 8260–8265.
[46] Yu, J. C.; Qian, C. G.; Zhang, Y. Q.; Cui, Z.; Zhu, Y.; Shen, Q. D.; Ligler, F. S.; Buse, J. B.; Gu, Z. Hypoxia and H_2O_2 dual-sensitive vesicles for enhanced glucose-responsive insulin delivery. *Nano Lett.*, **2017**, *17*, 733–739.
[47] Zhang, C.; Hong, S.; Liu, M. D.; Yu, W. Y.; Zhang, M. K.; Zhang, L.; Zeng, X.; Zhang, X. Z. pH-sensitive MOF integrated with glucose oxidase for glucose-responsive insulin delivery. *J. Control. Release*, **2020**, *320*, 159–167.

[48] Wu, W. T.; Mitra, N.; Yan, E. C. Y.; Zhou, S. Q. Multifunctional hybrid nanogel for integration of optical glucose sensing and self-regulated insulin release at physiological pH. *ACS Nano*, **2010**, *4*, 4831–4839.
[49] Volpatti, L. R.; Matranga, M. A.; Cortinas, A. B.; Delcassian, D.; Daniel, K. B.; Langer, R.; Anderson, D. G. Glucose-responsive nanoparticles for rapid and extended self-regulated insulin delivery. *ACS Nano*, **2020**, *14*, 488–497.
[50] Zhou, K. J.; Wang, Y. G.; Huang, X. N.; Luby-Phelps, K.; Sumer, B. D.; Gao, J. M. Tunable, ultrasensitive pH-responsive nanoparticles targeting specific endocytic organelles in living cells. *Angew. Chem., Int. Ed.*, **2011**, *50*, 6109–6114.
[51] Lončar, N.; Fraaije, M. W. Catalases as biocatalysts in technical applications: current state and perspectives. *Appl. Microbiol. Biotechnol.* , **2015**, *99*, 3351–3357.
[52] Chen, G. J.; Chen, Z. T.; Wen, D.; Wang, Z. J.; Li, H. J.; Zeng, Y.; Dotti, G.; Wirz, R. E.; Gu, Z. Transdermal cold atmospheric plasma-mediated immune checkpoint blockade therapy. *Proc. Natl. Acad. Sci. USA*, **2020**, *117*, 3687–3692.